Multiple conformational switches in a GTPase complex control co-translational protein targeting

Xin Zhang[a], Christiane Schaffitzel[b,1], Nenad Ban[b], and Shu-ou Shan[a,2]

[a]Division of Chemistry and Chemical Engineering, California Institute of Technology, 1200 East California Boulevard, Pasadena, CA 91125; and [b]Institute of Molecular Biology and Biophysics, ETH Zurich, 8093 Zurich, Switzerland

Edited by Jennifer A. Doudna, University of California, Berkeley, CA, and approved December 22, 2008 (received for review August 28, 2008)

The ''GTPase switch'' paradigm, in which a GTPase switches between an active, GTP-bound state and an inactive, GDP-bound state through the recruitment of nucleotide exchange factors (GEFs) or GTPase activating proteins (GAPs), has been used to interpret the regulatory mechanism of many GTPases. A notable exception to this paradigm is provided by two GTPases in the signal recognition particle (SRP) and the SRP receptor (SR) that control the co-translational targeting of proteins to cellular membranes. Instead of the classical ''GTPase switch,'' both the SRP and SR undergo a series of discrete conformational rearrangements during their interaction with one another, culminating in their reciprocal GTPase activation. Here, we show that this series of rearrangements during SRP-SR binding and activation provide important control points to drive and regulate protein targeting. Using real-time fluorescence, we showed that the cargo for SRP—ribosomes translating nascent polypeptides with signal sequences—accelerates SRP·SR complex assembly over 100-fold, thereby driving rapid delivery of cargo to the membrane. A series of subsequent rearrangements in the SRP·SR GTPase complex provide important driving forces to unload the cargo during late stages of protein targeting. Further, the cargo delays GTPase activation in the SRP·SR complex by 8–12 fold, creating an important time window that could further improve the efficiency and fidelity of protein targeting. Thus, the SRP and SR GTPases, without recruiting external regulatory factors, constitute a self-sufficient system that provides exquisite spatial and temporal control of a complex cellular process.

conformational change | fluorescence spectroscopy | protein targeting and translocation | signal recognition particle

SRP-mediated co-translational protein targeting delivers roughly one-third of proteins to their correct subcellular destinations, including the eukaryotic endoplasmic reticulum and the bacterial plasma membrane. This pathway involves a sequential series of molecular steps (1–3), including (*i*) recognition and loading of cargo (ribosomes translating nascent polypeptides with signal sequences) on the SRP; (*ii*) delivery of cargo to the target membrane via complex formation between SRP and SR; (*iii*) unloading and transfer of cargo from the SRP to the protein conducting channel (PCC); and (*iv*) disassembly of the SRP·SR complex and recycling of free SRP and SR for subsequent rounds of protein targeting. Like many cellular processes, this complex series of molecular interactions are spatially and temporally regulated by members of the GTPase superfamily, in this case, two highly homologous and directly interacting GTPases in both the SRP and SR.

SRP and SR provide a notable exception to the "GTPase switch" paradigm established for classical signaling GTPases (4). These GTPases do not exhibit substantial conformational changes depending on whether GTP or GDP is bound (5–7), and further, their intrinsic nucleotide exchange rates are 10^2–10^4-fold faster than those of classical GTPases (8, 9). Thus, no external GEFs are required to switch these GTPases from the GDP- to the GTP-bound state, and the facilitation of nucleotide exchange by an external GEF cannot be the mechanism to turn these GTPases to the "on" state. Moreover, both the SRP and SR reciprocally stimulate each other's GTP hydrolysis activity when they form a complex with one another (8, 10). Thus, no external GAPs are required either to switch these GTPases from the GTP- to the GDP-bound state, and the stimulation of GTP hydrolysis by an external GAP cannot be the mechanism to turn these GTPases to the "off" state. In contrast, these GTPases undergo a series of discrete conformational changes driven by heterodimeric interactions between the two GTPases (Fig. 1; ref. 10–13). Both proteins, starting in an inactive, "*open*" conformation, quickly bind one another to form a transient "*early*" intermediate independently of GTP (Fig. 1 *step 1*; ref. 14, 15). The presence of GTP bound at both GTPase active sites induces a conformational rearrangement in both proteins to form a stable "*closed*" complex (Fig. 1 *step 2*; ref. 11, 13, 16). A subsequent rearrangement involving the activation loops in both proteins activates GTP hydrolysis (Fig. 1 *step 3*; ref. 11, 12), which drives disassembly of the complex (Fig. 1 *step 4*; ref. 17).

If these conformational rearrangements during SRP·SR binding and activation are integral to the regulatory role of these GTPases in protein targeting, then they should be responsive to the biological events they are monitoring. To test this hypothesis, we examined the effects of cargo loading on the kinetic and thermodynamic features of the SRP and SR GTPase cycle. Our results demonstrate that the SRP and SR GTPases can use each of the conformational changes during their binding and activation cycle to sense temporal cues, such as cargo loading, and, in response, substantially change the free energy landscape of the different conformational states in the SRP·SR GTPase complex. These cargo-induced responses allow these GTPases to drive the efficient delivery and unloading of cargo to the target membrane, and to potentially improve the fidelity of protein targeting via kinetic proofreading mechanisms.

Results

General Experimental Approach. To monitor the different conformational stages of the SRP·SR complex, we used fluorescence resonance energy transfer (FRET) between donor and acceptor probes incorporated on both the SRP and SR. FRET provides a highly sensitive assay that allows us to detect the transient *early* intermediate (Fig. 1; ref. 14). Further, this intermediate can be distinguished from the subsequent conformations because it has a lower FRET value than the *closed* and *activated* complexes (Fig. 1; ref. 14). In addition, an environmentally sensitive probe, acrylodan, labeled at residue 235 of the SRP, detects formation of the *closed*

Author contributions: X.Z. and S.-o.S. designed research; X.Z. and S.-o.S. performed research; X.Z., C.S., and N.B. contributed new reagents/analytic tools; X.Z. and S.-o.S. analyzed data; and X.Z. and S.-o.S. wrote the paper.

The authors declare no conflict of interest.

This article is a PNAS Direct Submission.

[1]Present address: Grenoble Outstation, European Molecular Biology Laboratory and Unit of Virus Host-Cell Interactions, UJF-EMBL-CNRS, UMR 5233, 6 rue Jules Horowitz, BP181, 38042 Grenoble Cedex 9, France.

[2]To whom correspondence should be addressed. E-mail: sshan@caltech.edu.

This article contains supporting information online at www.pnas.org/cgi/content/full/0808573106/DCSupplemental.

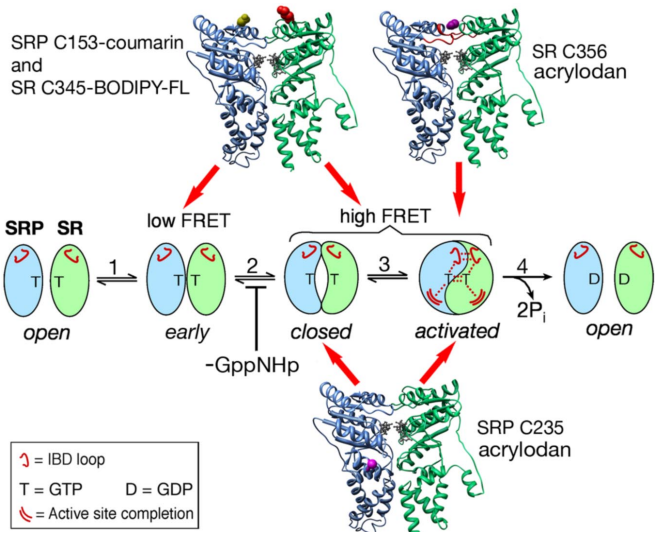

Fig. 1. Multiple conformational changes during SRP·SR complex formation and activation (11, 14), as described in the text, and the positions of fluorescence probes that detect the different conformational stages, as described in the text.

and *activated* complexes but not the *early* intermediate (Fig. 1 and Fig. S1), thereby simplifying kinetic and thermodynamic analyses of these later conformations. Finally, acrylodan labeled at residue 356 of the SR near its catalytic loop specifically detects the *activated* complex (Fig. 1 and Fig. S2). In addition to these fluorescent probes, mutant GTPases and GTP analogues were used to block specific rearrangements and thus isolate each conformational intermediate (10, 11). We can block the *early*→*closed* rearrangement by leaving out GTP (Fig. 1; ref. 14); this allows us to isolate the *early* intermediate and characterize its kinetics and stability. Mutations in the catalytic loop, SRP A144W or SR A335W, allow a stable *closed* complex to form but block its rearrangement to the *activated* complex (11, 18). The nonhydrolyzable GTP analogue 5′-guanylylimido-diphosphate (GppNHp) allows most of the rearrangements to occur but inhibits GTP hydrolysis (10, 11). Using these tools, we determined how the SRP and SR GTPases use their conformational changes to respond to cargo loading.

Cargo Accelerates Assembly of a Stable SRP·SR Complex over 100-fold. As cargo, we purified stalled ribosome-nascent chain complexes (RNCs) bearing the N-terminal 74 aa of the model SRP substrate FtsQ (19–21). SRP·SR complex assembly was monitored using FRET in the presence of GppNHp. Comparison of the time courses for complex assembly shows 3 differences between free and cargo-loaded SRP (Fig. 2*A*): (*i*) the initial rates are much faster with cargo-loaded SRP; (*ii*) the kinetics of complex formation with cargo-loaded SRP is bi-phasic with a burst phase, suggesting the accumulation of an intermediate; (*iii*) at completion of the reaction, FRET plateaus at a lower value for cargo-loaded SRP, suggesting a change in the equilibrium stability of the final SRP·SR complex. These effects are further characterized below.

An observed rate constant for complex formation (k_{obsd}) at any protein concentration is the sum of the complex assembly and disassembly rate constants (Eq. 1; 22)

$$k_{\mathrm{obsd}} = k_{\mathrm{on}} \times [\mathrm{SR}] + k_{\mathrm{off}} \qquad [1]$$

To isolate the effect of cargo on complex assembly, we measured the observed rate constants as a function of SR concentration; the slope of this concentration dependence gives the association rate constant, k_{on} (Eq. **1**; Fig. 2*B*). The value of k_{on} is 4.4×10^4 M^{-1}·s^{-1} in the absence of cargo, consistent with previous measurements (10). In the presence of cargo, the complex formation rate constant

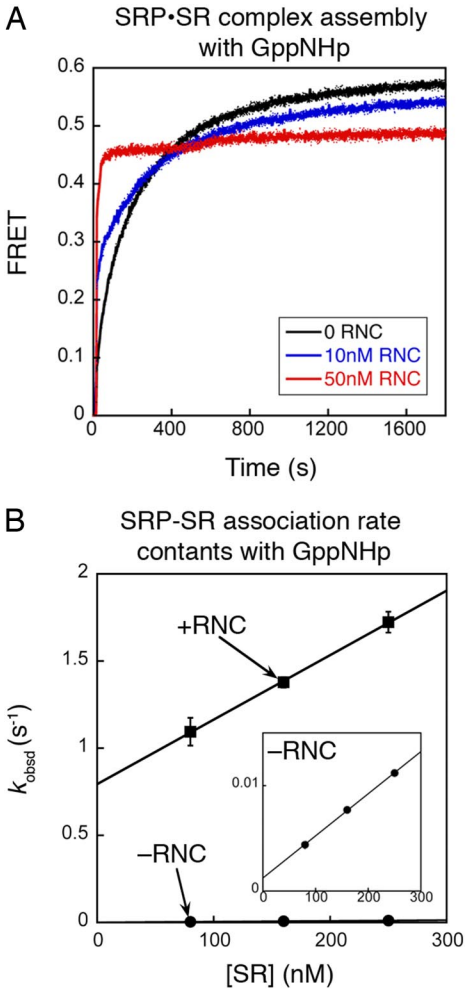

Fig. 2. Cargo changes the kinetics of SRP–SR interaction. (*A*) Time courses for SRP·SR complex assembly with GppNHp in the absence (black) or presence of 10 nM (blue) and 50 nM (red) RNC, using 10 nM SRP and 100 nM SR to mimic physiological protein concentrations (23). (*B*) Cargo accelerates SRP·SR complex assembly with GppNHp by 100-fold. The data are fit to Eq. **1** and gave association rate constants (k_{on}) of $3.7 \pm 0.4 \times 10^6$ M^{-1}·s^{-1} and $4.0 \pm 0.3 \times 10^4$ M^{-1}·s^{-1} with (■) and without (●) 60 nM RNC, respectively.

is 100–400-fold faster (Fig. 2*B* and *SI Text* Fig. S3A). Thus, the cargo-loaded SRP has a substantial kinetic advantage over the free SRP to form a complex with the SR, ensuring efficient delivery of cargo to the target membrane.

Cargo Stabilizes the *Early* Intermediate by Two Orders of Magnitude. The biphasic kinetics with a burst phase during complex formation with cargo-loaded SRP suggests the accumulation of an intermediate (Figs. 2*A* and 3*A*, blue). A likely candidate to account for this burst is the *early* intermediate, which forms quickly and has a lower FRET value than the subsequent complexes (Fig. 1; ref. 14). To test this notion, we blocked the *early*→*closed* rearrangement and isolated the *early* complex by performing complex assembly in the absence of nucleotide (Figs. 1 *step 2* and 3*A*, green). Both the rate and the magnitude of FRET changes for assembly of the *early* intermediate agree well with those of the burst phase during complex assembly with GppNHp (Fig. 3*A*). This provides strong evidence that in the presence of cargo, the *early* intermediate accumulates substantially during complex assembly.

The *early* intermediate, which lacks stabilizing interactions from the γ-phosphate of GTP, is very unstable without cargo (5, 14), hence it cannot accumulate under the nanomolar concentrations of

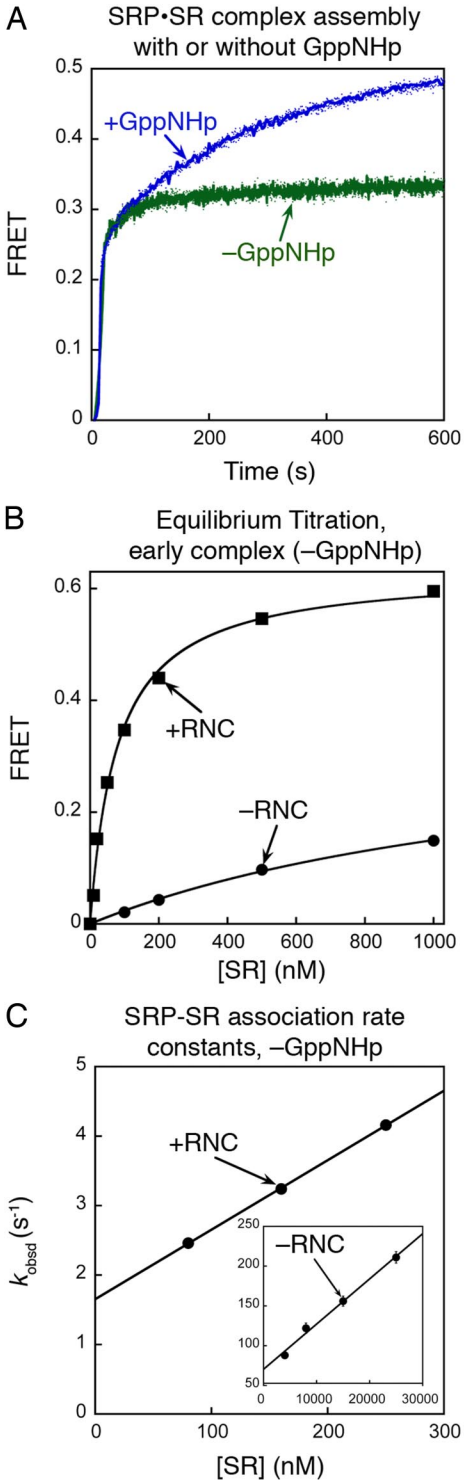

Fig. 3. Cargo stabilizes the early intermediate. (*A*) Comparison of the time courses for SRP·SR complex formation for cargo-loaded SRP in the absence (green) and presence of 100 μM GppNHp (blue). Data were obtained using 20 nM SRP, 100 nM SR, and 20 nM RNC. (*B*) Cargo stabilizes the *early* intermediate 50-fold. Equilibrium titration of the *early* complex assembled in the absence of GppNHp with (■) and without (●) 50 nM RNC. Nonlinear fits of data gave K_d values of 80 ± 4 nM in the presence of RNC. (*C*) Cargo increases the kinetic stability of the *early* intermediate 40-fold. The data are analyzed as in part *B* and give $k_{on} = 1.0 \pm 0.1 \times 10^7\ M^{-1}{\cdot}s^{-1}$ with cargo-loaded SRP, which is within two-fold of the value in the absence of RNC ($k_{on} = 5.6 \pm 0.3 \times 10^6\ M^{-1}{\cdot}s^{-1}$) (14), and $k_{off} = 1.62 \pm 0.1\ s^{-1}$, which is 40-fold slower than that in the absence of RNC ($k_{off} = 60 \pm 2\ s^{-1}$) (14). The inset shows the data in the absence of RNC (adapted from ref. 14). Note the difference in scales between the two plots.

SRP and SR used here (Fig. 2*A*, black). Therefore, it was surprising to detect its accumulation with cargo-loaded SRP. This observation suggests that the cargo strongly stabilizes this intermediate. To test this hypothesis, we determined the equilibrium and kinetic stability of the *early* complex with and without cargo. Indeed, the cargo stabilizes the *early* complex over 50-fold, lowering its equilibrium dissociation constant (K_d) from 4–10 μM (14) to 80 ± 4 nM (Fig. 3*B*, squares) and decreasing its dissociation rate constant (k_{off}, derived from the y-intercept in Fig. 3*C*) from 62 ± 2 s^{-1} to 1.6 ± 0.1 s^{-1}.

Stabilization of the *early* intermediate explains the faster rate of SRP·SR complex assembly with GppNHp for cargo-loaded SRP (Fig. 2*B*). Without cargo, formation of the highly labile *early* intermediate is not sufficient to give a stable SRP·SR complex; to obtain a stable complex, the *early* intermediate needs to rearrange to the *closed* complex. However the *early* intermediate dissociates quickly and less than 2% of the population rearranges to form the *closed* complex ($k_{off} = 62 \pm 2\ s^{-1}$ vs. $k_{rearrange} = 1.03 \pm 0.02\ s^{-1}$; ref. 14). This gives rise to the slow rate constant for formation of a stable *closed* complex between free SRP and SR. In contrast, for cargo-loaded SRP the *early* intermediate is stabilized over 50-fold. Thus forming the *early* complex (Fig. 1 *step 1*) is sufficient to give a relatively stable SRP·SR complex under physiological SRP and SR concentrations (200–400 nM; ref. 23). Furthermore, the cargo·SRP·SR *early* complex dissociates with much slower kinetics (Fig. 3*C*, $k_{off} = 1.6 \pm 0.1\ s^{-1}$), giving this intermediate a much longer lifetime to undergo subsequent rearrangements. Both of these effects contribute to the faster rate of assembling a stable GTPase complex with cargo-loaded SRP in the presence of GppNHp.

Cargo Stalls the SRP·SR Complex at Earlier Conformational Stages. The different FRET end points in Fig. 2*A* suggest that the stability of the final SRP·SR complex is also altered by the cargo. To test this hypothesis, we compared the equilibrium stability of the SRP·SR complex assembled in GppNHp with and without cargo using SRP C235 labeled with acrylodan (Fig. 1 and Fig. S1). Equilibrium titrations using this probe showed that the cargo destabilizes the *closed*/*activated* complexes four-fold, increasing its K_d from 10 ± 2 nM to 40 ± 4 nM (Fig. 4*A*). A similar destabilizing effect was observed using the FRET probes, with the K_d of the *closed*/*activated* complexes increasing from 14 ± 3 nM without cargo to 60 ± 7 nM with cargo-loaded SRP (*SI Text* Fig. S4). An additional probe that specifically monitors the *activated* complex, acrylodan-labeled SR C356 (Fig. 1 and Fig. S2), also confirmed that the cargo destabilizes the *activated* complex (Fig. 4*B*). In summary, the results from all three fluorescence probes showed that, in contrast to the large stabilizing effect of the cargo on the *early* intermediate, the subsequent conformations during the SRP–SR interaction are destabilized by the cargo.

Thus the cargo significantly alters the conformational rearrangements in the SRP·SR complex (Fig. 4*C*). Without cargo, the *closed* and *activated* states are >400-fold more stable than the *early* intermediate, therefore the equilibrium for the *early*→*closed* rearrangement is extremely favorable (Fig. 4*C*, K^{rel} = 400–1000). In contrast, in the cargo·SRP·SR complex, this rearrangement is 200-fold less favorable (Fig. 4*C*, K^{rel} = 1.3–22). Thus, in the cargo·SRP·SR complex, a substantial fraction of the GTPase complex is still in the *early* conformation (30–40%) even in the presence of GppNHp. This conformational heterogeneity of the GTPase complex in the presence of cargo is consistent with previous EM analysis that showed that, whereas the SRP is well-resolved in the RNC·SRP complex, upon addition of the SR and GppNHp, the electron density for both the SRP and SR GTPase domains are no longer visible (24). Thus, both the biochemical and structural analyses highlight the dynamic nature of the GTPase complex when it is bound to the cargo.

The SRP·SR complex can use the *early*→*closed* rearrangement to

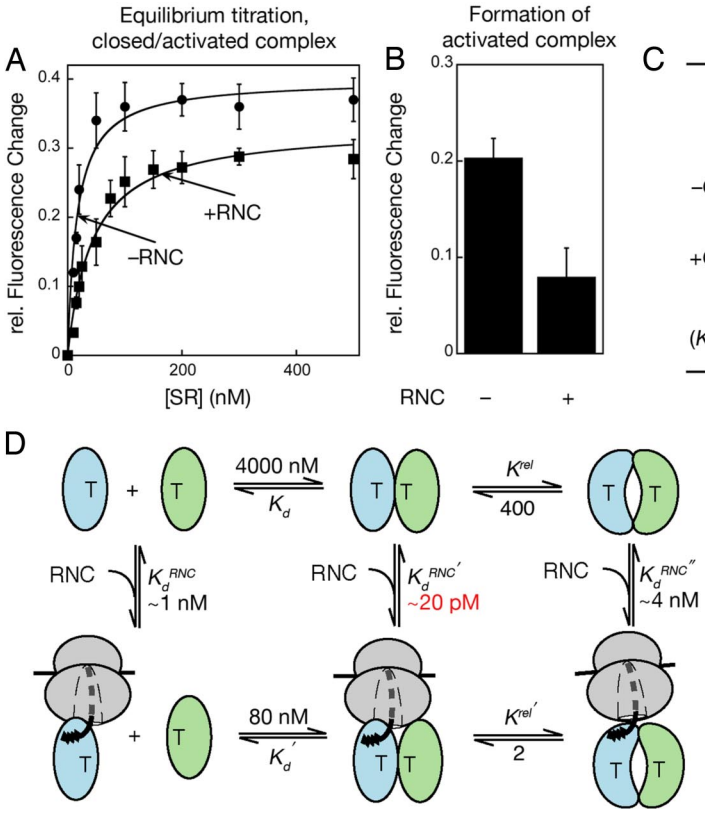

	K_d	
	– RNC	+ RNC
–GppNHp	4-10 μM	80 nM
+GppNHp	10 nM	40 nM
K^{rel} (K_d^{-G}/K_d^{+G})	400-1000	2

Fig. 4. Cargo destabilizes the *closed* and *activated* states during SRP·SR interaction. (*A*) Equilibrium titration of the SRP·SR complex assembled in GppNHp with (■) and without (●) RNC using acrylodan-labeled SRP C235. Nonlinear fits of data gave K_d values of 10 ± 2 nM (without RNC) and 40 ± 4 nM (with RNC). (*B*) Relative fluorescence changes of acrylodan-labeled SR C356 in the presence and absence of cargo, obtained using 50 nM SRP and 15 nM labeled SR with 100 μM GppNHp. An accurate K_d value could not be determined with this probe because of the large amount of cargo-loaded SRP that would be required to saturate labeled SR C356. (*C*) Equilibrium constants of the GTP-independent (K_d^{-G}) and GTP-dependent (K_d^{+G}) SRP·SR complexes with or without RNC. The equilibrium for rearrangement (K^{rel}) were calculated from $K^{rel} = K_d^{-G}/K_d^{+G}$. (*D*) Thermodynamic analysis of the interaction of cargo with SRP at different conformational stages during the SRP–SR interaction.

drive cargo unloading during protein targeting (Fig. 4*D*). Initially, cargo loading stabilizes the *early* intermediate 50-fold (Fig. 4*D*, K_d and K_d'). Correspondingly, the interaction of cargo with the SRP should be stabilized to the same extent in the *early* intermediate (Fig. 4*D*, $K_d^{RNC\prime}/K_d^{RNC} = K_d'/K_d = 50$). Using the K_d^{RNC} value of ~ 1 nM (25, 26), the stability of cargo bound to the *early* intermediate ($K_d^{RNC\prime}$) to be 20 pM. Although this effect could enhance the initial recognition and delivery of cargo to the membrane, such strong binding will block the subsequent unloading of cargo from the SRP. This problem is circumvented by the 200-fold destabilizing effect of cargo on the *early*→*closed* rearrangement (Figs. 4*C* and *D*, K^{rel} and $K^{rel\prime}$). Correspondingly, the interaction of cargo with the SRP would also be weakened 200-fold by this rearrangement (Fig. 4*C*, $K_d^{RNC\prime\prime}/K_d^{RNC} = K^{rel\prime}/K^{rel}$), thus priming the cargo for subsequent unloading. This model is supported by mutational analyses that showed that mutant GTPases defective in the *early*→*closed* rearrangement severely block protein translocation (18). The observation that mutants defective in the *closed*→*activated* rearrangement inhibit protein translocation further suggests that this last rearrangement is also essential for cargo unloading (18). Therefore, both rearrangements within the GTPase complex provide essential driving forces to help unload the cargo from the SRP to the PCC, thus initiating protein translocation.

Because cargo disfavors the rearrangements to form the *activated* complex, one would predict that stimulated GTP hydrolysis, which occurs from the *activated* complex, would also be impaired. To test this notion, we compared the GTPase reaction rate from the SRP·SR complex in the presence and absence of cargo. In the absence of cargo, the GTPase rate of free SRP is significantly stimulated by the addition of the SR (Fig. 5, circles). The reaction rate reaches a plateau of 0.79 s^{-1} at saturating SR concentrations, representing the GTPase rate constant from the SRP·SR complex (Fig. 5, circles). In the presence of cargo, significantly less GTPase stimulation was observed (Fig. 5, squares). Intriguingly, two plateaus were observed for the GTPase reaction in the presence of cargo (Fig. 5, squares), suggesting the presence of two populations of cargo·SRP·SR complexes: one population, which forms at low SR concentrations (below 50 nM), hydrolyzes GTP at a rate constant of 0.064 s^{-1}; the second population, which forms at higher SR concentrations (above 1 μM), hydrolyzes GTP at a rate constant of 0.11 s^{-1} (Fig. 5, squares). Although the nature of this heterogeneity is unclear at present, in both of these populations the GTPase activity is repressed by the RNC (12- and 8-fold for the first and second populations, respectively). The effect of cargo in reducing the GTP hydrolysis rate is specific to the SRP·SR complex as the cargo does not affect the basal GTP hydrolysis rate of the free SRP (*SI Text* Fig. S5). Thus the cargo also delays GTPase activation in

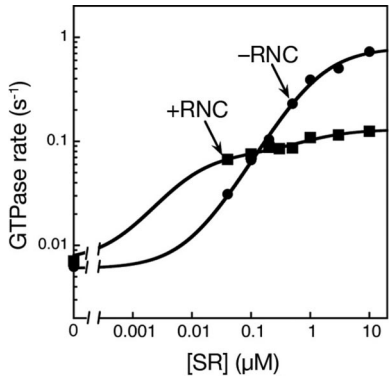

Fig. 5. Cargo delays activation of GTP hydrolysis in the SRP·SR complex. GTPase rate constants were measured using 40 nM SRP and 100 μM GTP in the absence (■) and presence (●) of 100 nM RNC. The data in the absence of cargo were fit to a single binding curve and gave a rate constant of 0.79 s^{-1} for GTP hydrolysis from the SRP·SR complex. The data in the presence of cargo is not consistent with a single binding curve and was fit to a model based on two populations of SRP·SR complexes that reacts at rate constants of 0.064 and 0.11 s^{-1}.

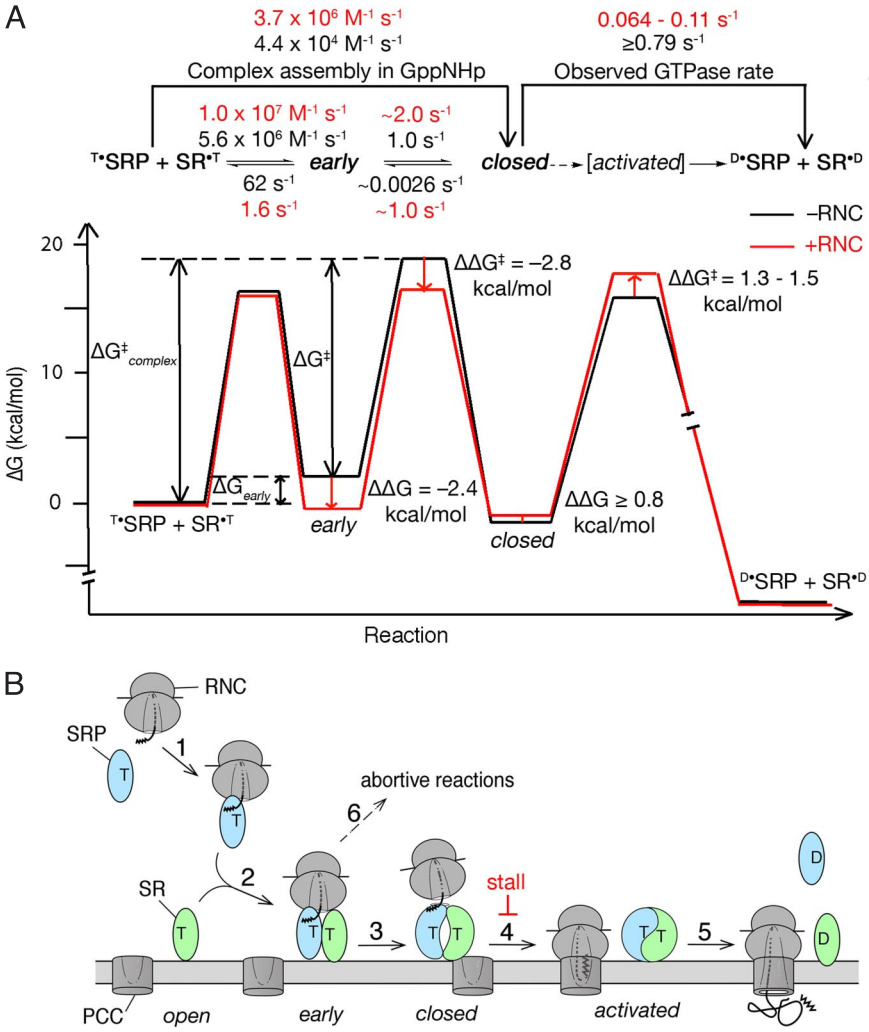

Fig. 6. Conformational changes during the SRP–SR interaction respond to cargo loading and regulate protein targeting. (*A*) Rate constants and free energy profiles for the SRP–SR interaction in the absence (black) and presence (red) of cargo. A standard state of 200 nM SRP is used to approximate cellular protein concentrations. Activation energies were calculated from the observed association and dissociation rate constants using $\Delta G^{\ddagger} = -RT\ln(kh/k_BT)$, where R = 1.987 cal·K^{-1}·mol^{-1}, $h = 1.58 \times 10^{-37}$ kcal·s^{-1}, $k_B = 3.3 \times 10^{-27}$ kcal·K^{-1}, and T = 298K. The relative energies of the different complexes were calculated from the observed equilibrium stabilities using $\Delta G = -RT\ln K$, where K is the equilibrium constant. ΔG_{early} is the free energy cost to form the *early* complex, $\Delta G^{\ddagger}$ is the activation energy for the *early*→*closed* rearrangement. The sum of these two gives the overall energy barrier to form the *closed* complex ($\Delta G^{\ddagger}_{complex}$), which is lowered 2.8 kcal·mol^{-1} by the cargo. In contrast, the RNC increases the activation energy for GTP hydrolysis by 1.3–1.5 kcal·mol^{-1}. (*B*) Proposed model for how the conformational changes during the SRP–SR interaction regulate protein targeting and translocation as described in text.

the SRP·SR complex. This effect, which we term "stalling," would provide an important time window that allows the SRP to unload the cargo before GTP hydrolysis drives irreversible complex disassembly, as discussed below.

Discussion

We showed here that cargo loading substantially alters the free energy landscape of the SRP–SR interaction cycle (Fig. 6*A*). Without cargo (black), assembly of a stable SRP·SR complex is slow because it requires rearrangement from an unstable *early* intermediate [Fig. 6*A*, $\Delta G^{\ddagger}_{complex} = \Delta G_{early} + \Delta G^{\ddagger}$; (14)]. Further, the stable SRP·SR complex has a short lifetime because as soon as it is formed, rapid activation of GTP hydrolysis drives its irreversible disassembly (8). The cargo uses a remarkably simple solution to these problems, by stabilizing the *early* intermediate (Fig. 6*A*, $\Delta\Delta G = -2.4$ kcal/mol) and disfavoring the *closed* and *activated* states (Fig. 6*A*, $\Delta\Delta G \geq +0.8$ kcal/mol). This accelerates complex assembly (Fig. 6A, $\Delta\Delta G^{\ddagger} = -2.8$ kcal/mol), and prolongs the lifetime of the SRP·SR complex because of delayed GTP hydrolysis (Fig. 6*A*, $\Delta\Delta G^{\ddagger} = +1.3$–$1.5$ kcal/mol). The rate-limiting step of the SRP–SR interaction cycle changes from the *early*→*closed* rearrangement with free SRP to GTP hydrolysis with cargo-loaded SRP.

These cargo-induced effects allow the SRP and SR to use each of their conformational rearrangements to regulate a distinct step during protein targeting (Fig. 6*B*). At the beginning of each targeting cycle, cargo loading (Fig. 6*B step 1*) allows the SRP to assemble a stable complex with SR >100-fold faster (Fig. 6*B step 2*). This ensures rapid delivery of cargo to the membrane (15, 27) and avoids futile interactions between the free SRP and SR. In the *early* intermediate, the cargo is locked in the SRP·SR complex with very high affinity (Fig. 4*D*, $K_d^{RNC'} \sim 20$ pM), allowing the SRP to effectively compete with cellular chaperones for binding the cargo. Subsequent GTPase rearrangements to the *closed* and *activated* conformations weaken the interaction of cargo with the SRP (Fig. 6*B steps 3* and *4*; *cf.* Fig. 4*D*) and thus help the SRP to switch from a cargo-binding mode to a cargo-release mode, to unload the cargo to the PCC (Fig. 6*B step 4*). Once in the *activated* conformation, and especially after cargo release, rapid GTP hydrolysis drives the disassembly and recycling of both the SRP and SR (Fig. 6*B step 5*).

The mechanism proposed here (Fig. 6*B*) focuses on the GTP-bound SRP and SR because the high cellular concentration of GTP compared to GDP (~900 μM and 100 μM in bacteria, respectively) predicts that over 90% of both GTPases are bound with GTP. Minor pathways are also possible in which empty-site or GDP-bound forms of the SRP and SR first form the *early* intermediate to deliver cargo to the membrane surface, followed by rapid binding or exchange of GTP to drive the subsequent steps (15, 27); these pathways are not depicted in Fig. 6*B* for clarity.

The most intriguing effect of cargo is "stalling," that is, the delay of GTPase activation by ~8–12-fold (Fig. 6*B step 4*). A similar effect was suggested from studies of the mammalian system where before the addition of the PCC, a stable cargo·SRP·SR complex persists in the presence of GTP, suggesting that the cargo may also delay GTP hydrolysis in the mammalian SRP·SR complex (28). We suggest

that stalling creates an important time window during which the SRP ensures the efficiency and fidelity of protein targeting via either or both of the following mechanisms. First, stalling could provide a spatial checkpoint for the target membrane and/or the PCC. Before the SR associates with the PCC, stalling prevents premature GTP hydrolysis that would irreversibly disassemble the SRP·SR complex and thus help avoid abortive targeting reactions (Fig. 6*B step 6*). Interaction of SR with the PCC may trigger the rearrangement to the *closed* and *activated* states and initiate cargo unloading (28). The PCC also competes with the SRP for interacting with the RNC (20, 21, 24, 29), which could further drive the transfer of cargo from the SRP to the PCC (28, 30). Alternatively or in addition, stalling could provide a fidelity checkpoint. Many of the effects of the cargo described here are observed only with RNCs but not with empty ribosomes (*SI Text* Fig. S6), establishing the importance of the signal sequence. It could be envisioned that cargos with weaker signal sequences could not effectively stall the SRP·SR complex, and thus are more likely to be rejected via premature GTP hydrolysis (Fig. 6*B step 6*). In this way, GTP hydrolysis could be used to improve the fidelity of protein targeting akin to kinetic proofreading mechanisms used by elongation factor GTPases (31).

Materials and Methods

Materials. The *Eschericia coli* SRP and SR GTPases (Ffh and FtsY, respectively) and 4.5S RNA were expressed and purified using established procedures (8, 18). Most of the fluorescence experiments used the FtsY (47–497) construct. This truncated FtsY construct behaves similarly to full length FtsY in its ability to interact with the SRP and to respond to the cargo (*SI Text* Fig. S3). The GTPase reactions with and without cargo was determined with full length FtsY. Mutant proteins were constructed using the QuikChange procedure (Stratagene), and were expressed and purified by the same procedure as that for the wild-type protein. Fluorescent dyes DACM, BODIPY-FL, and acrylodan were from Invitrogen. 70S ribosomes and RNCs were purified as described previously (19, 32) and in the *SI Text*.

Fluorescence Labeling. For FRET measurements, maleimide derivatives of coumarin and BODIPY-FL were used to label single-cysteine mutants of the SRP and SR, respectively, as described (14). Labeling of the SRP and SR with acrylodan followed the same procedure except that the labeling reaction was carried out using a 30-fold excess of dye over protein for over 12 h at 4 °C. Absorbance of acrylodan (ε_{391} = 20,000 $M^{-1}\cdot cm^{-1}$) was used to determine the concentration of labeled protein. The efficiency of labeling reaction was typically greater than or equal to 90% for both proteins. The background, estimated from the labeling of the SRP and SR lacking cysteines using the same procedure, is less than 3%.

Fluorescence Measurement. All measurements were carried out at 25 °C in assay buffer [50 mM KHEPES, pH 7.5, 150 mM KOAc, 10 mM $Mg(OAc)_2$, 2 mM DTT, 0.01% Nikkol] on a Fluorolog-3 spectrofluorometer (Jobin Yvon) as described (8, 14). FRET measurements were carried out using an excitation wavelength of 380 nm and an emission wavelength of 470 nm. FRET efficiency was calculated as described (14). Fluorescence emission spectrum of the SRP (or SR) labeled with acrylodan was measured using an excitation wavelength of 370 nm. Fluorescence emission at 500 nm was monitored for equilibrium titrations using acrylodan-labeled protein.

Pulse–chase experiments were carried out using unlabeled protein to trap any dissociated SRP or SR (10). Fast reactions were measured on a Kintek stop-flow apparatus (10). The incubation time during equilibrium measurements was calculated based on the SRP·SR complex assembly rate (10, 14), and varies from 5 min for fast reactions (*early* complex assembly and complex assembly in the presence of cargo) to several hours (complex assembly with GppNHp in the absence of cargo).

GTPase Assay. The GTPase assay to measure the stimulated GTP hydrolysis reaction between the SRP and SR were carried out and analyzed as described (8). Multiple turnover reactions were carried out at 25 °C with a small, fixed amount of free or cargo-loaded SRP and increasing concentrations of SR; 100 μM GTP (doped with trace γ-^{32}P-GTP) was present in the reaction to saturate both GTPase sites. The data presented in Fig. 5 was representative of four experiments. Previous studies have established that the GTPase reaction rate is rate-limited by SRP·SR complex formation at sub-saturating SR concentrations, whereas at saturating SR concentrations, the reaction is rate-limited by GTP hydrolysis or a slow conformational change preceding GTP hydrolysis (8). The release of products, including dissociation of GDP, P_i, and disassembly of the GDP·SRP·SR·GDP complex, are not rate-limiting in this GTPase assay (8).

ACKNOWLEDGMENTS. We thank Sandra Schmid, Douglas C. Rees, Raymond Deshaies, Nathan Pierce, and members of the Shan laboratory for comments on the manuscript. This work was supported by a National Institutes of Health grant GM078024 to S.S., and by the Swiss National Science Foundation (SNSF) and the NCCR Structural Biology program of the SNSF to N.B. S.S. was supported by a career award from the Burroughs Welcome Foundation, the Henry and Camille Dreyfus foundation, the Beckman Young Investigator award, and the Packard and Lucile award in science and engineering. X.Z. was supported by a fellowship from the Ulric B. and Evelyn L. Bray Endowment Fund.

1. Walter P, Johnson AE (1994) Signal sequence recognition and protein targeting to the endoplasmic-reticulum membrane. *Annu Rev Cell Biol* 10:87–119.
2. Matlack KES, Mothes W, Rapoport TA (1998) Protein translocation: Tunnel vision. *Cell* 92:381–390.
3. Johnson AE, van Waes MA (1999) The translocon: A dynamic gateway at the ER membrane. *Annu Rev Cell* Dev Biol 15:799–842.
4. Bourne HR (1986) GTP-binding proteins: One molecular machine can transduce diverse signals. *Nature* 321:814–816.
5. Focia PJ, Gawronski-Salerno J, Coon JS, Freymann DM (2006) Structure of a GDP:AlF_4 complex of the SRP GTPases Ffh and FtsY, and identification of peripheral nucleotide interaction site. *J Mol Biol* 360:631–643.
6. Freymann DM, Keenan RJ, Stroud RM, Walter P (1999) Functional changes in the structure of the SRP GTPase on binding GDP and Mg^{2+}GDP. *Nat Struct Biol* 6:793–801.
7. Freymann DM, Keenan RJ, Stroud RM, Walter P (1997) Structure of the conserved GTPase domain of the signal recognition particle. *Nature* 385:361–364.
8. Peluso P, Shan SO, Nock S, Herschlag D, Walter P (2001) Role of SRP RNA in the GTPase cycles of Ffh and FtsY. *Biochemistry* 40:15224–15233.
9. Jagath JR, Rodnina MV, Lentzen G, Wintermeyer W (1998) Interaction of guanine nucleotides with the signal recognition particle from *Escherichia coli*. *Biochemistry* 37:15408–15413.
10. Peluso P, *et al.* (2000) Role of 4.5S RNA in assembly of the bacterial signal recognition particle with its receptor. *Science* 288:1640–1643.
11. Shan SO, Stroud RM, Walter P (2004) Mechanism of association and reciprocal activation of two GTPases. *PLoS Biol* 2:1572–1581.
12. Egea PF, *et al.* (2004) Substrate twinning activates the signal recognition particle and its receptor. *Nature* 427:215–221.
13. Shan SO, Walter P (2003) Induced nucleotide specificity in a GTPase. *Proc Natl Acad Sci USA* 100:4480–4485.
14. Zhang X, Kung S, Shan SO (2008) Demonstration of a multistep mechanism for assembly of the SRP·SRP receptor complex: Implications for the catalytic role of SRP RNA. *J Mol Biol* 381:581–593.
15. Rapiejko PJ, Gilmore R (1997) Empty site forms of the SRP54 and SRα GTPases mediate targeting of ribosome nascent chain complexes to the endoplasmic reticulum. *Cell* 89:703–713.
16. Lu Y, *et al.* (2001) Evidence for a novel GTPase priming step in the SRP protein targeting pathway. *EMBO J* 20:6724–6734.
17. Miller JD, Wilhelm H, Gierasch L, Gilmore R, Walter P (1993) GTP-binding and hydrolysis by the signal recognition particle during initiation of protein translocation. *Nature* 366:351–354.
18. Shan SO, Chandrasekar S, Walter P (2007) Conformational changes in the GTPase modules of the signal reception particle and its initiation of protein translocation. *J Cell Biol* 178:611–620.
19. Schaffitzel C, Ban N (2007) Generation of ribosome nascent chain complexes for structural and functional studies. *J Struct Biol* 158:463–471.
20. Mitra K, *et al.* (2005) Structure of the *E coli* protein-conducting channel bound to a translating ribosome. *Nature* 438:318–324.
21. Schaffitzel C, *et al.* (2006) Structure of the *E coli* signal recognition particle bound to a translating ribosome. *Nature* 444:503–506.
22. Fersht A (1999) in *Structure and mechanism in protein science: a guide to enzyme catalysis and protein folding*, (W.H. Freeman, New York), pp 143.
23. Jensen CG, Pedersen S (1994) Concentrations of 4.5S RNA and Ffh protein in *Escherichia coli*: The stability of Ffh protein is dependent on the concentration of 4.5S RNA. *J Bacteriol* 176:7148–7154.
24. Halic M, *et al.* (2006) Signal recognition particle receptor exposes the ribosomal translocon binding site. *Science* 312:745–747.
25. Bornemann T, Jockel J, Rodina MV, Wintermeyer W (2008) Signal sequence-independent membrane targeting of ribosomes containing short nascent peptides within the exit tunnel. *Nat Struct Mol Biol* 15:494–499.
26. Flanagan JJ, *et al.* (2003) Signal recognition particle binds to ribosome-bound signal sequences with fluorescence-detected subnanomolar affinity that does not diminish as the nascent chain lengthens. *J Biol Chem* 278:18628–18637.
27. Bacher G, Lutcke H, Jungnickel B, Rapoport TA, Dobberstein B (1996) Regulation by the ribosome of the GTPase of the signal-recognition particle during protein targeting. *Nature* 381:248–251.
28. Song WQ, Raden D, Mandon EC, Gilmore R (2000) Role of Sec61α in the regulated transfer of the ribosome-nascent chain complex from the signal recognition particle to the translocation channel. *Cell* 100:333–343.
29. Halic M, *et al.* (2006) Following the signal sequence from ribosomal tunnel exit to signal recognition particle. *Nature* 444:507–511.
30. Pool MR, Stumm J, Fulga TA, Sinning I, Dobberstein B (2002) Distinct modes of signal recognition particle interaction with the ribosome. *Science* 297:1345–1348.
31. Rodnina MV, Wintermeyer W (2001) Fidelity of aminoacyl-tRNA selection on the ribosome: Kinetic and structural mechanisms. *Annu Rev Biochem* 70:415–435.
32. Moazed D, Noller HF (1989) Interaction of tRNA with 23S rRNA in the ribosomal A, P, and E sites. *Cell* 57:585–597.